Electronic Supplementary Material (ESI) for Nanoscale.

SUPPORTING INFORMATION

Versatile thiolactone-based conjugation strategies to polymer stabilizers for multifunctional UCNP nanohybrid aqueous dispersions

Izabela Kurowska,[a,b,c] Baptiste Amouroux,[b] Marvin Langlais,[b] Olivier Coutelier,[b] Christophe Coudret,[b]
Mathias Destarac[b,*] and Jean-Daniel Marty[b,*]

[a] Faculty of Chemistry, University of Bialystok, Ciołkowskiego 1k, 15-245 Bialystok, Poland
[b] IMRCP, CNRS UMR 5623, Université de Toulouse, 31062 Toulouse Cedex 09, France
[c] Doctoral School of Exact and Natural Sciences, University of Bialystok, Ciołkowskiego 1k, 15-245 Bialystok, Poland

A. Synthesis and characterization of polymers.

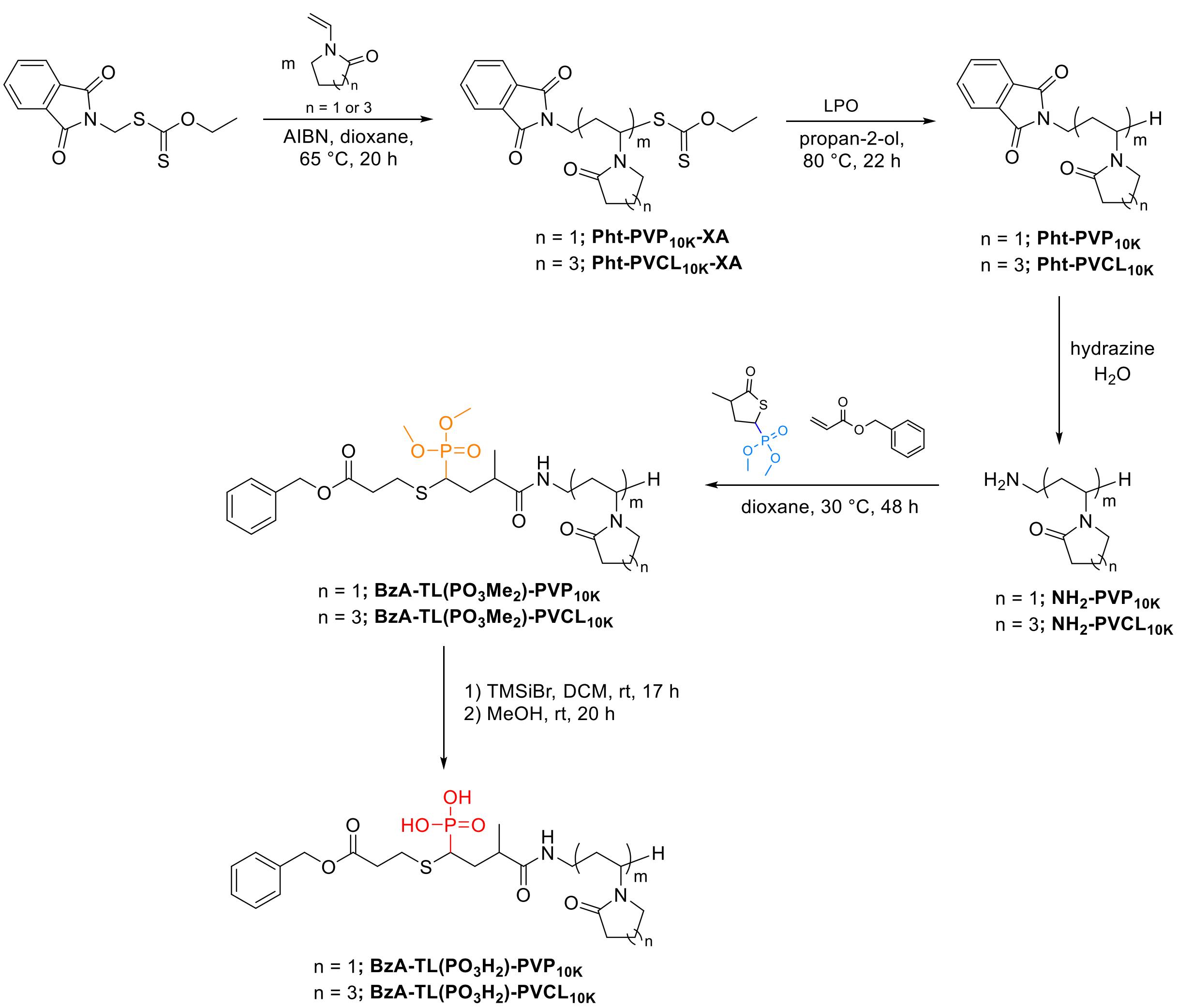

n = 1; **Pht-PVP$_{10K}$-XA**
n = 3; **Pht-PVCL$_{10K}$-XA**

n = 1; **Pht-PVP$_{10K}$**
n = 3; **Pht-PVCL$_{10K}$**

n = 1; **NH$_2$-PVP$_{10K}$**
n = 3; **NH$_2$-PVCL$_{10K}$**

n = 1; **BzA-TL(PO$_3$Me$_2$)-PVP$_{10K}$**
n = 3; **BzA-TL(PO$_3$Me$_2$)-PVCL$_{10K}$**

n = 1; **BzA-TL(PO$_3$H$_2$)-PVP$_{10K}$**
n = 3; **BzA-TL(PO$_3$H$_2$)-PVCL$_{10K}$**

Scheme S1. Synthetic approach for the synthesis of phosphonic acid-containing poly(*N*-vinylpyrrolidinone) or poly(*N*-vinylcaprolactam) using RAFT polymerization and thiolactone chemistry.

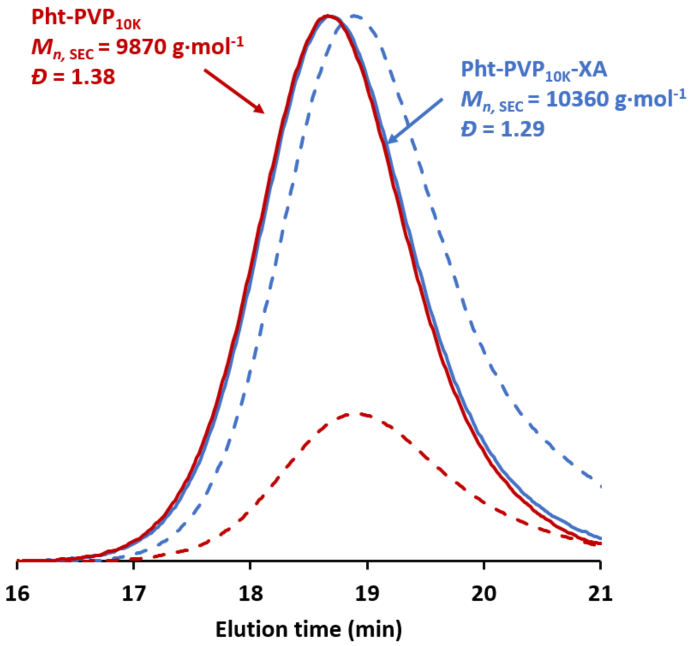

Figure S1. SEC-RI (solid traces) and SEC-UV (dashed traces, λ = 290 nm) chromatograms of Pht-PVP$_{10K}$-XA (blue traces) obtained by RAFT polymerization and Pht-PVP$_{10K}$ (red traces) obtained after reduction of the xanthate ω-end group.

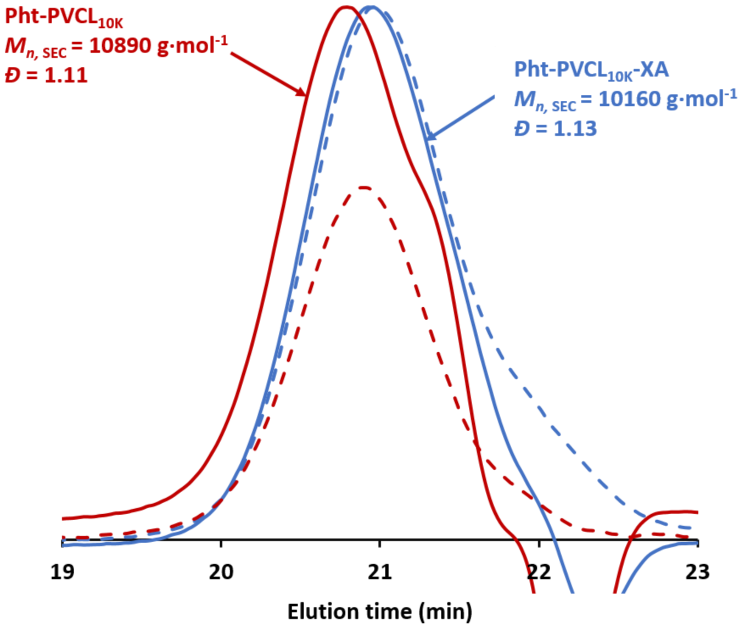

Figure S2. SEC-RI (solid traces) and SEC-UV (dashed traces, λ = 290 nm) chromatograms of Pht-PVCL$_{10K}$-XA (blue traces) obtained by RAFT polymerization and Pht-PVCL$_{10K}$ (red traces) obtained after reduction of the xanthate ω-end group.

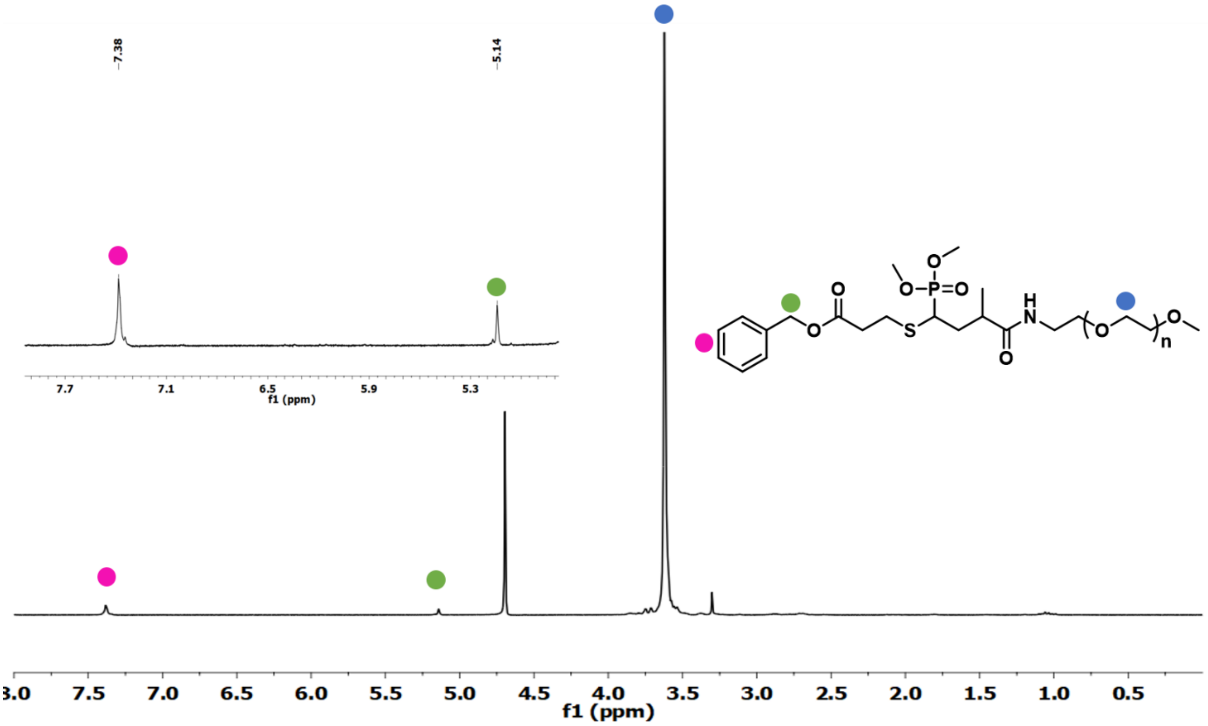

Figure S3. ^{1}H NMR spectrum of BzA-TL(PO_3Me_2)-PEG_{2K} (300.13 MHz, D_2O, 298K).

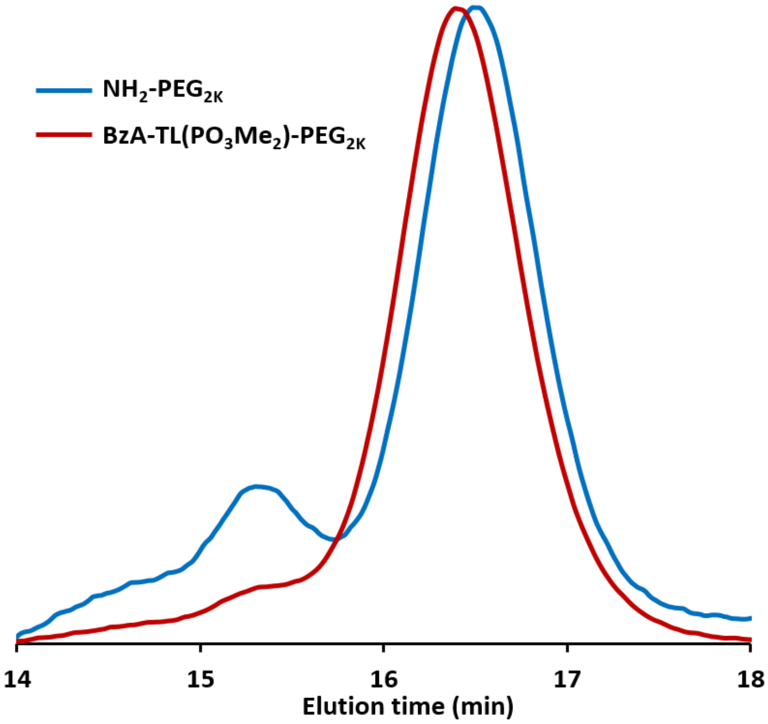

Figure S4. SEC-RI chromatograms of NH_2-PEG_{2K} (blue trace) and BzA-TL(PO_3Me_2)-PEG_{2K} (red trace) obtained after chain-end functionalization using thiolactone.

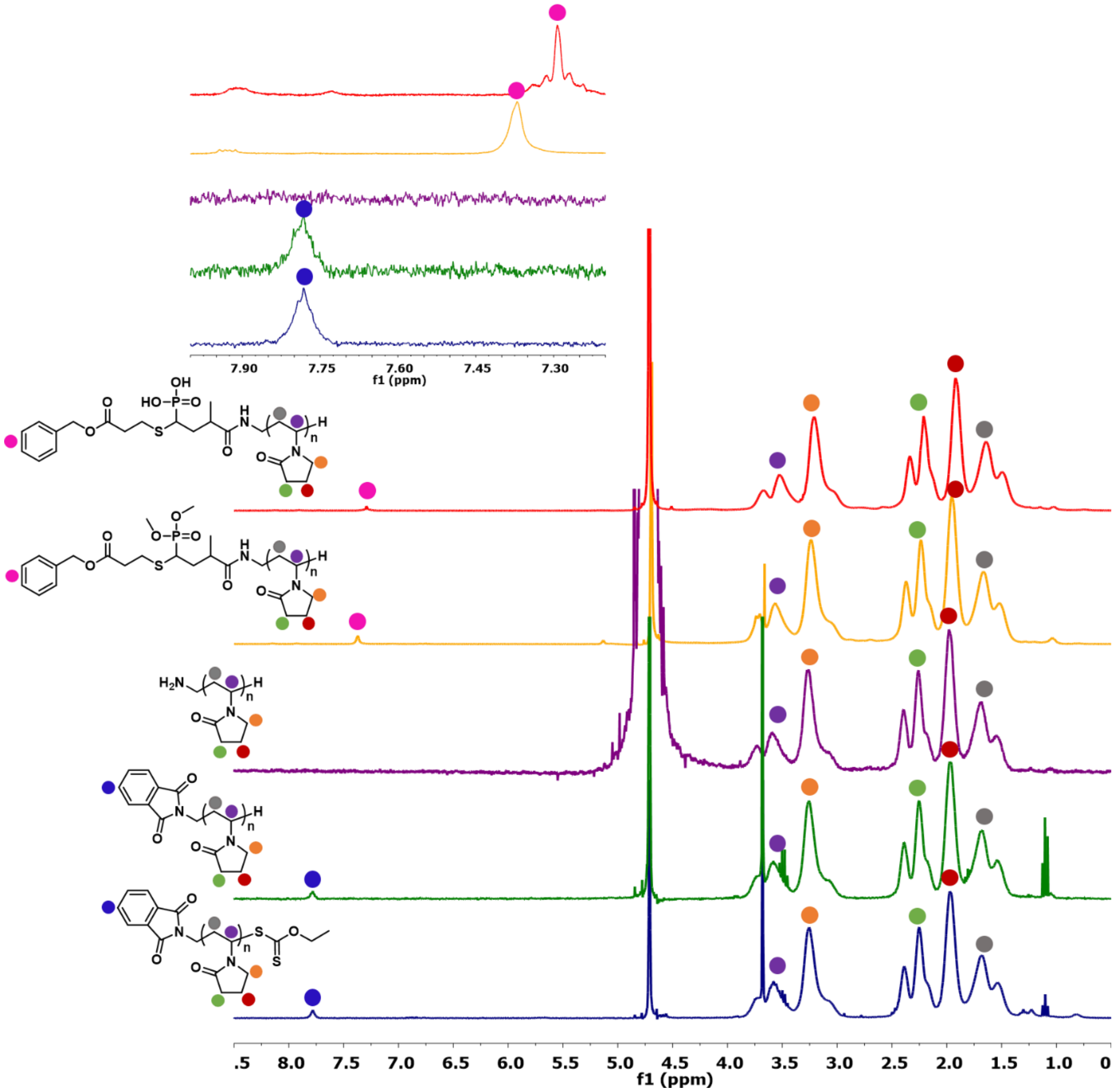

Figure S5. Comparison of ^1H NMR spectra for PVP modifications (300.13 MHz, D_2O, 298K).

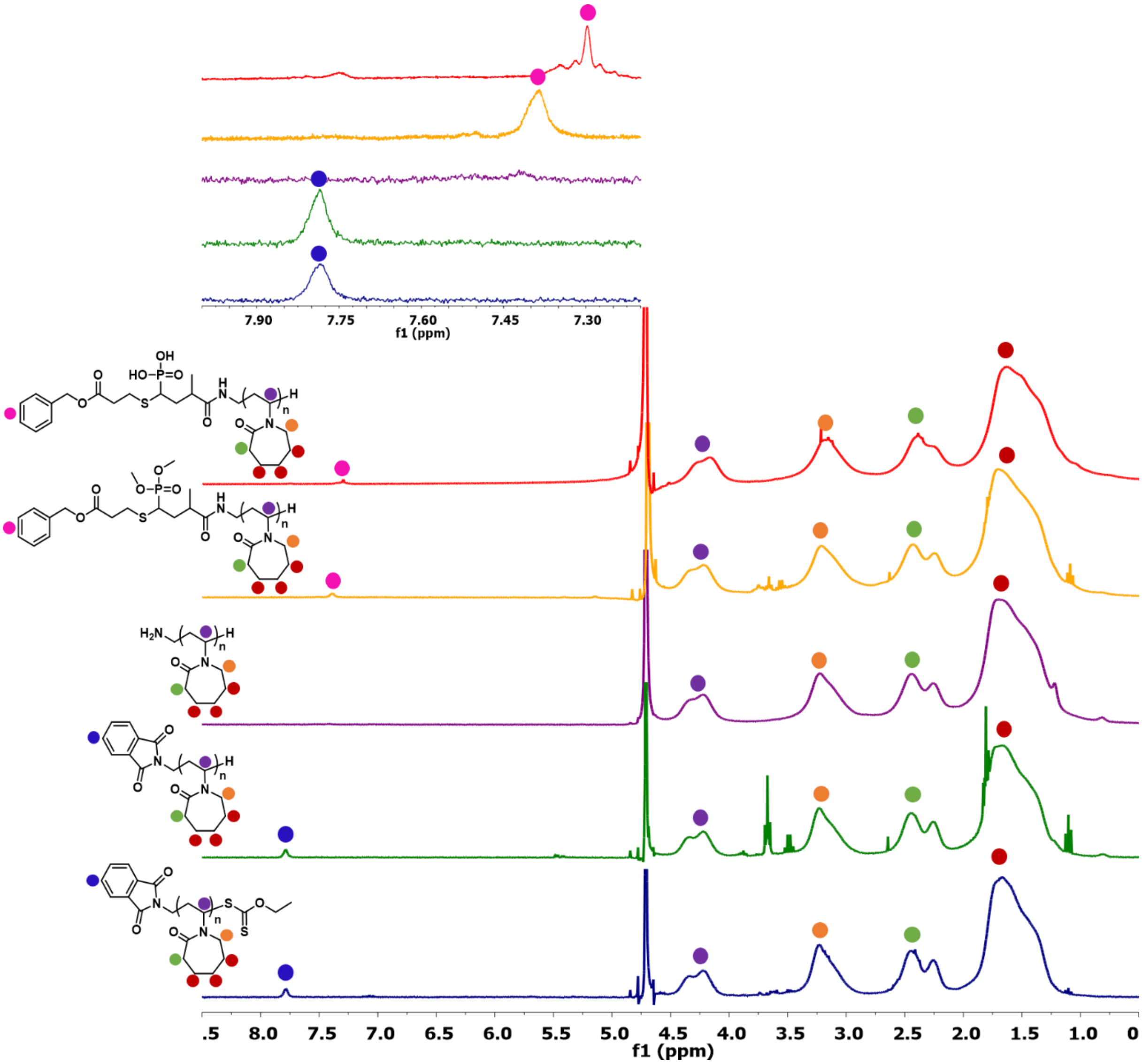

Figure S6. Comparison of ^{1}H NMR spectra for PVCL modifications (300.13 MHz, D_2O, 298K).

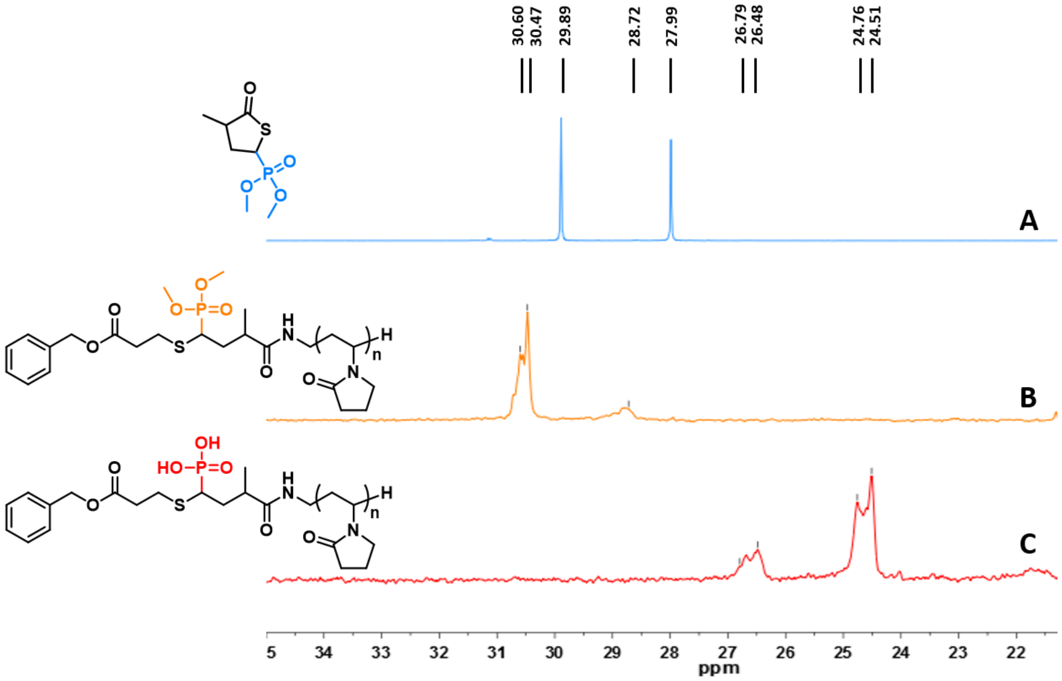

Figure S7.^{31}P NMR spectra of **(A)** thiolactone (Dimethyl(4-methyl-5-oxotetrahydothiophen-2-yl)phosphonate), **(B)** BzA-TL(PO_3Me_2)-PVP$_{10K}$, and **(C)** BzA-TL(PO_3H_2)-PVP$_{10K}$ (121,49 MHz, D_2O, 298K).

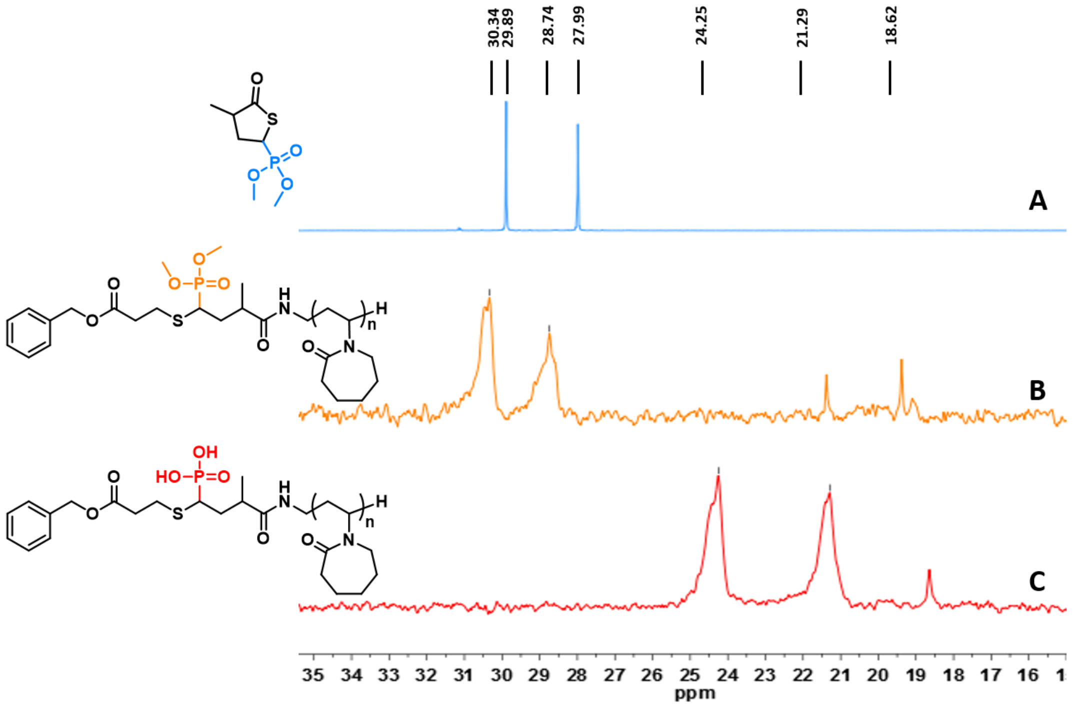

Figure S8.^{31}P NMR spectra of **(A)** thiolactone (Dimethyl(4-methyl-5-oxotetrahydothiophen-2-yl)phosphonate), **(B)** BzA-TL(PO_3Me_2)-PVCL$_{10K}$, and **(C)** BzA-TL(PO_3H_2)-PVCL$_{10K}$ (121,49 MHz, D_2O, 298K).

B. Synthesis and characterization of UCNPs.

B.1. Preparation of 20nm NaYF$_4$ UCNP nanoparticles. NaYF$_4$ UCNPs co-doped by 30%Yb and 1%Tm were prepared by using the most user-friendly protocol of Zhang *et al.*[1] As reported in our previous paper[2], sodium (9.31 mmol NaOH, 16 mL MeOH) and fluoride (12.8 mmol NH$_4$F, 16 mL MeOH) precursors were introduced simultaneously *in situ* via the use of dual syringe pumps to the NaREF$_4$@oleate solution (2.33 mmol).

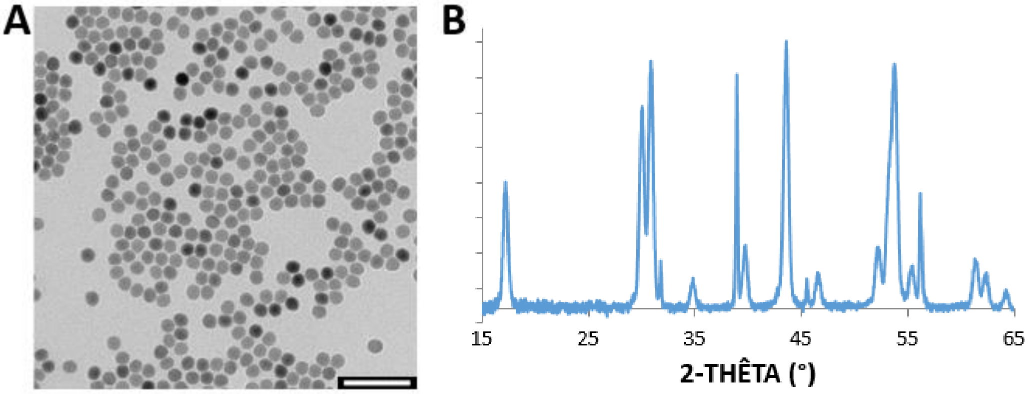

Figure S9. Characterization of NaYF$_4$ UCNPs prepared. A and B are respectively TEM picture (scale bar is 100 nm) and XRD diffractogram. This batch of NaYF$_4$-based UCNPs shows a size diameter 20±2.6 nm and pure β-phase as attested by XRD diffractograms.

B.2. Synthesis of ultrasmall UCNPs (<6 nm). Ultrasmall core and core@shell UCNPs were prepared following protocols established by Amouroux *et al.*[3] In the present work, all the experiments with ultrasmall UCNPs concern only core@shell UCNPs. The cores were just an intermediate reactant to produce the ultrasmall core@shell.

Preparation of core UCNP nanoparticles: Na(Yb$_{20\%}$Gd$_{79\%}$)F$_4$:Tm$_{1\%}$. NaGdF$_4$:Yb,Tm cores were prepared following our previous reported microwave synthesis, using 2mmol lanthanides (79%Gd, 20%Yb; 1%Tm)[2], where the high temperature microwave heating plateau was replaced by 6 successive cycles of heat pulses with an Anton Paar Monowave300 reactor: 1 min a 300°C followed by 5 min at 285°C. The last cycle ended with a fast cooling down step to room temperature. Eventually, UCNPs were purified by 3 washing in EtOH and centrifugation (9000 RPM for 10 min) before storage in cyclohexane at 50 mg·mL^{-1}.

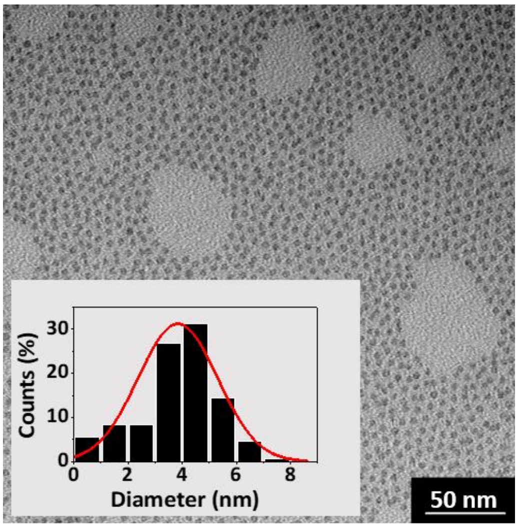

Figure S10. TEM image of the Na($Yb_{20\%}Gd_{79\%}$)F_4:$Tm_{1\%}$ core and corresponding size distribution (3,8 ± 1,5 nm).

Preparation of core@shell UCNPs: Na($Yb_{20\%}Gd_{79\%}$)F_4:$Tm_{1\%}$@$NaGdF_4$. $NaGdF_4$ shell growth was achieved via trifluoroacetate pyrolysis following synthesis protocol described by Zhai *et al.,*[4] 2 mmol of $GdCl_3$ (1eq) were introduced in 40 mL of oleic acid(OA)/octadec-1-ene (ODE) 1/1. After Gd(oleate)$_3$ formation, the totality of the cores UCNPs and 5 mmol of sodium trifluoroacetate (8 mL MeOH) were introduced at room temperature. The final high temperature heating step from Zhai *et al.* was replaced by a 300°C plateau during 15 min with an Anton Paar Monowave300 microwave reactor, similarly to our previously reported core synthesis.[2]

C. Modification of preformed UCNPs by ligand exchange mechanism: towards multifunctional materials.

C.1. Theoretical background of Dynamic Light scattering (DLS).

DLS analysis was used to extract Z-average values, derived count rate, intensity and number average distributions for each studied nano-object sample. In order to give a critical view on the results issued from these analyses, a brief overview of the assumptions relative to these is given below.

From auto-correlation function to self-diffusion coefficient D. Particles in suspension (without sedimentation or creaming) undergo random Brownian motion with a characteristic (translational) diffusion coefficient D, which is related to the size and shape of the objects (see below). Under laser illumination, this motion induces a random fluctuation of the light scattered by the particles. The temporal behavior of the intensity of the scattered light contains therefore information on the particles' size and shape. To extract this information, analysis through auto-correlation of the scattered intensity signal could be performed. The auto-correlation intensity function $G(\tau,q)$ is defined as followed :

$$G(\tau,q) = \langle I(t,q).I(t+\tau,q)\rangle / \langle I(t,q)\rangle^2 \qquad \textbf{(1)}$$

with <> denotes the integral of the function versus the time t
τ the delay time,
q the scattering vector $q = 4\pi\, n/\lambda_o \sin(\theta/2)$ with λ_o the incident laser wavelength, θ the scattering angle and n the optical index of the solution.

In the following parts, we suppose that each photon is scattered only once before being detected i.e. the solutions are diluted enough. When multiple scattering occurs, the results below are no longer correct.

In the case of *monodisperse and non-interacting nanoparticles,* $G(\tau,q)$ is following a single exponential decay:

$$G(\tau,q) = A.(1+\beta.[e^{-\Gamma.\tau}]^2) \qquad \textbf{(2)}$$

with A the measured baseline,
β a parameter depending on the coherence optics,
Γ is a decay rate, which is equal to $q^2.D$.

Fitting the auto-correlation function of the experimental scattered intensity leads therefore to an estimation of the diffusion coefficient. Then, the size of the particle may be estimated from D after making assumption on the shape of the object. In the simple case of spherical particles, one will use the Stokes-Einstein equation:

$$R_h = k_B T/(6\pi\eta D) \text{ (Stokes Einstein)} \qquad \textbf{(3)}$$

with R_h the hydrodynamic radius,
η the viscosity of the solution at the temperature T,
k_B the Boltzmann constant.

Note that the hydrodynamic radius is influenced by any changes of the nanoparticles surface structure or concentration of ions in the medium and that any mistake on the used viscosity and optical index values induces an important error on the calculated R_h. For anisotropic objects, the single exponential decay of the auto-correlation function is still observed for not so long objects (typically less than 150 nm).

Furthermore, the normalized average quantity of photon reaching the correlator (**Derived count rate** in the Malvern software) is a valuable indication to avoid misinterpretation issued from the single analysis of auto-correlation function. A low value for this quantity indicates either a too low concentrated sample or the absence of significant amount of colloidal structures within solution. It also renders the treatment of auto-correlation function more risky as the level of relative noise is dramatically increased.

In the case of *polydisperse and non-interacting nanoparticles,* the auto-correlation intensity function $G(\tau,q)$ no longer follows a single exponential decay but should be based on a sum or an integral over a distribution $F(\Gamma)$ of the diffusion coefficient:

$$G(\tau,q) = A.(1+\beta.[\int_0^\infty F(\Gamma).e^{-\Gamma.\tau}\ d\Gamma\ ]^2) \quad \text{with} \quad \int_0^\infty F(\Gamma)\ d\Gamma = 1 \qquad \textbf{(5)}$$

Note that this distribution is over the decay rate not over the size of particles.
The main difficulty is now to extract from the experimental autocorrelation function, the distribution function $F(\Gamma)$. Two approaches can be used:

- if the distribution function is monomodal and narrow enough, one can use the cumulant analysis leading to the **Z-average diameter** and an estimate of the width of the distribution (**Polydispersity index PDI**).

- in the general case, one can estimate the distribution function by a discrete function. Fitting this function with the auto-correlation one will lead to a plot of the relative intensity of light scattered by particles in various size classes (**intensity size distribution**).

Determination of polydispersity by cumulant analysis. Using Taylor expansion and cumulants of the distribution function, one can demonstrate that the equation (5) leads to (Applied Optics 40(24) 4087 (2001):

$$G(\tau,q) = A(1+ \beta.e^{-2\bar{D}.q^2\tau}.\left(1+\frac{\mu_2}{2!}.\tau^2-\frac{\mu_3}{3!}.\tau^3 \ldots\right)^2) \qquad \textbf{(6)}$$

with $\bar{D}$ the average hydrodynamic diffusion coefficient,
μ_i the i th moment of the distribution function F defined as:
$\mu_i = \int_0^\infty F(\Gamma).(\Gamma - q^2.\bar{D})^i.d(\Gamma)$.

Fitting the experimental auto-correlation to the equation (6) by the least squares method gives easily:

- the average hydrodynamic diffusion coefficient which corresponds to the mean of the distribution $F(\Gamma)$, assuming a single peak Gaussian distribution. The equivalent hydrodynamical diameter (through the Stokes Einstein equation, with the hypothesis that the nanoparticle are spherical – i.e. micelles, vesicles, polymersomes etc…-) can then be calculated and is called the intensity weighted **Z-average mean diameter.** The Z-average mean diameter is the recommended value to be used in quality control (ISO standard document 13321:1996 E and 22412). If the sample is not a solution of monomodal, spherical and monodisperse nanoparticle, the Z-average size can only be used to compare various samples measured in the same dispersant and same conditions.
- the value second moment (μ_2) leads to the **polydispersity index** corresponding to the relative standard deviation of that distribution (PdI). In the case of a Gaussian distribution, this is directly the variance of the distribution. If estimated, the third moment (μ_3) provides a measure of the skewness or asymmetry of the distribution.

Fit of the correlation function by multiple exponential: intensity size distribution. For *samples with a multiple size distribution*, $G(\tau,q)$ is written as a discreet sum of exponential functions:

$$G(\tau,q) = A.(1+\beta.[\sum_i \alpha_i.e^{-\Gamma_i.\tau}\ d\Gamma\ ]^2) \qquad \textbf{(7)}$$

with α_i the intensity-weighted contribution of the Γ_i decay rate associated to particles having a diffusion coefficient of $D_i = \frac{\Gamma_i}{q^2}$. The intensity-weighted distribution is obtained from a deconvolution of the measured intensity autocorrelation function of the sample. Generally, this is accomplished by using a non-negatively constrained least squares (NNLS) fitting algorithm, common examples being CONTIN, General Purpose and Multiple Narrow Mode algorithms using a certain number of defined size classes. These different algorithms differed from each other by the level of noise which is kept before deconvolution process (also called regularization). Indeed, a small amount of noise in the correlation function can generate a large number of distributions. In the case of spherical homogeneous particles, the intensity-weighted particle size distribution is then obtained by using Stokes Einstein equation (3).

From intensity distribution to volume or number size distribution. The intensity distribution is naturally weighted according to the scattering intensity of each particle fraction or family. As such, the intensity distribution can be somewhat misleading, in that a small amount of aggregation or presence or a larger particle species can dominate the distribution. This distribution can be converted, using Mie theory, to a number distribution describing the relative proportion of multiple components in the sample based on their number rather than based on their scattering. Given the optical properties of the particle and the scattering angle, Mie theory estimates the scattering intensity M(x) as a function of particle diameter x, dispersant and particle optical properties. The discreet list of Γ_i decay rate associated weighted by α_i could be transformed into a list of radii R_i (assuming spherical particles) through the equation $D_i = \frac{\Gamma_i}{q^2} = k_B T/(6\pi\eta R_i)$ weighted by the coefficient $\alpha_l/M(R_i)$.

Alternatively, conversion can be roughly obtained by assuming that M(x) is proportional to R^6 (in the case of small homogeneous spheres – i.e. micelles but not vesicles or polymersomes -) which is only correct for particle below ca 100 nm of diameter. For vesicles or polymersomes, one may suppose that M(x) is proportional to $R^4.t^2$ where t is the thickness of the shell thickness. Note that the Mie theory implies that a particular model has been chosen to describe the particles (homogeneous, spheres, hollow spheres, coated spheres…).

When transforming an intensity distribution to a number distribution, different assumptions are used: *all particles are homogeneous and spherical*, *the optical properties of the particles are known and intensity distribution is correct*. Moreover DLS technique itself produces distributions with inherent peak broadening, so there will always be some error in the representation of the intensity distribution. As such, number distributions derived from these intensity distributions emphasizes information obtained from a small fraction of the collected data. Therefore they are best used for comparative purposes, or for estimating the relative proportions where there are multiple modes, or peaks, and should never be considered as absolute.

C.2. Experimental datas

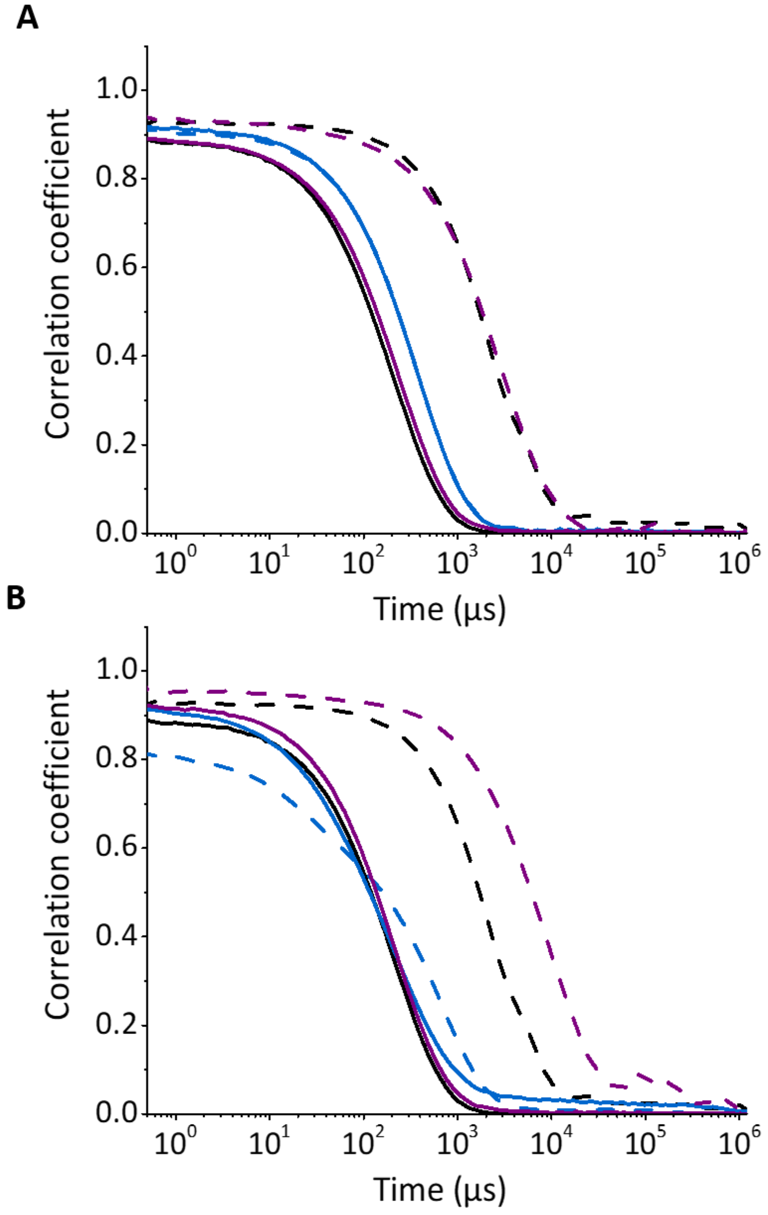

A.

Figure S11. A) Correlograms of UCNPs@BzA-TL(PO_3H_2)-PVP_{10K} (blue traces), UCNPs@NH_2-PVP_{10K} (violet traces), and UCNPs (black traces) solutions in the presence (dashed traces) or not (solid traces) of NaCl obtained from DLS experiments. **B)** Correlograms of UCNPs@BzA-TL(PO_3H_2)-$PVCL_{10K}$ (blue traces), UCNPs@NH_2-$PVCL_{10K}$ (violet traces), and UCNPs (black traces) solutions in the presence (dashed traces) or not (solid traces) of NaCl obtained from DLS experiments.

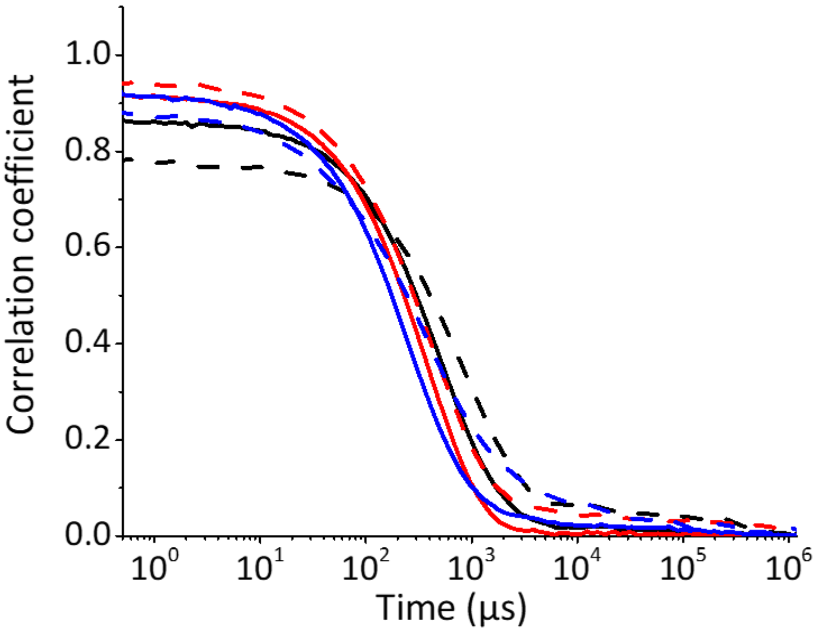

Figure S12. Correlograms of UCNPs@BzA-TL(PO_3H_2)-PEG_{2K} (black traces), UCNPs@BzA-TL(PO_3H_2)-PVP_{10K} (red traces), and UCNPs@BzA-TL(PO_3H_2)-$PVCL_{10K}$ (blue traces) solutions after dialysis in the presence (dashed traces) or not (solid traces) of NaCl obtained from DLS experiments.

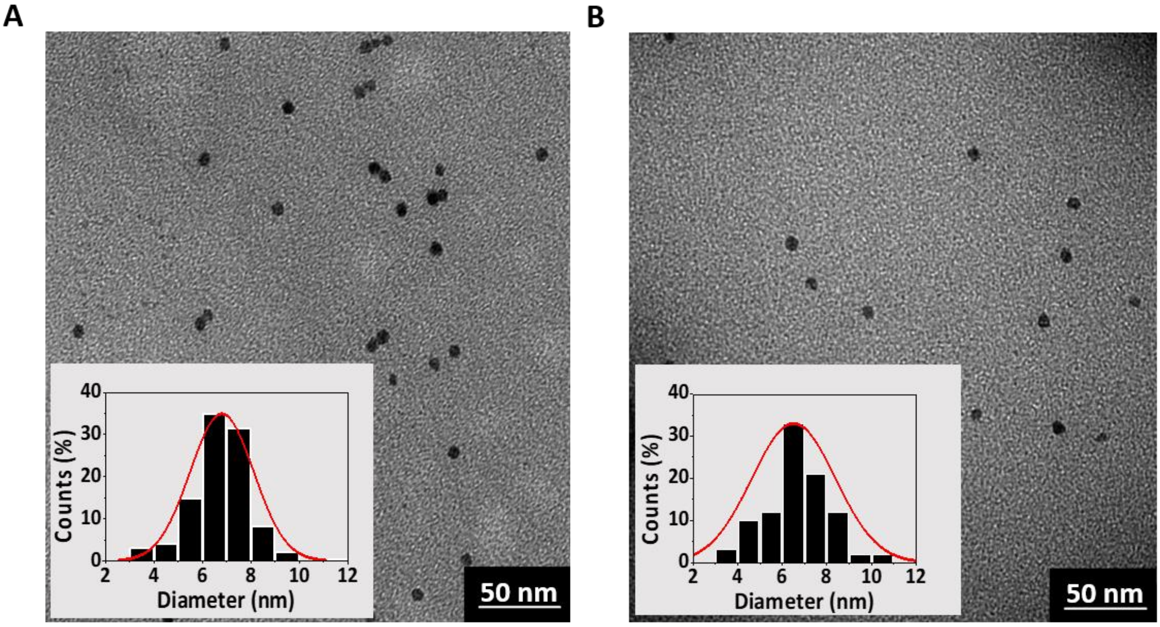

Figure S13. TEM image of UCNPs@polymer and corresponding size distribution: **(A)** UCNPs@BzA-TL(PO_3H_2)-PVP_{10K}, **(B)** UCNPs@BzA-TL(PO_3H_2)-$PVCL_{10K}$.

D. Quantitative approach of the polymer loading at the surface of a single UCNP

D.1. ^{1}H NMR

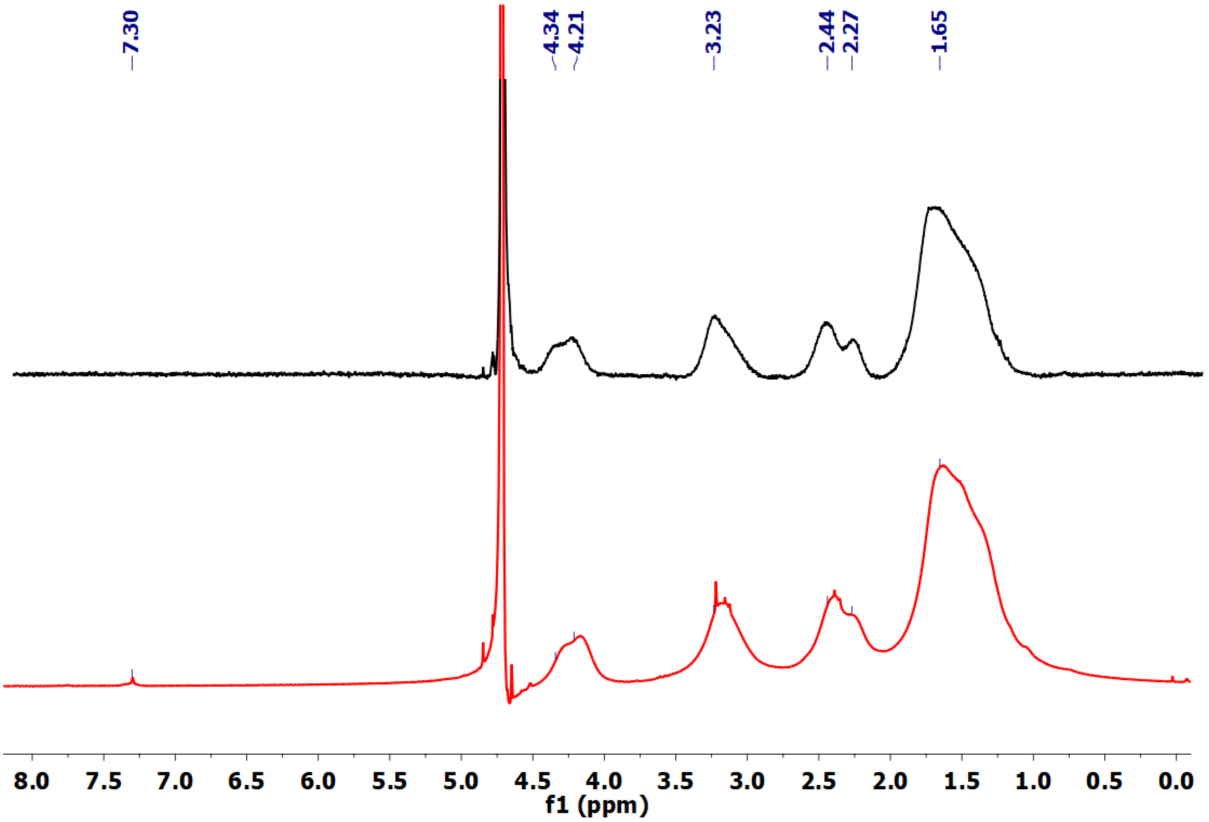

Figure S14. ^{1}H NMR spectra of BzA-TL(PO_3H_2)-PVCL$_{10K}$ (red) and the UCNPs@BzA-TL(PO_3H_2)-PVCL$_{10K}$ (black), (300.13 MHz, D_2O, 298K).

D.2. Quantitative ^{31}P NMR

Table S1. Details on the solutions used for the quantitative NMR (volume, concentration, mole)

	Unit	value	Error σ
[cyclophosphamide]	mol/L	2.041×10^{-3}	0.033×10^{-3}
V(cyclophosphamide)	mL	0.425	0.004
n(cyclophosphamide)	Mol	8.66×10^{-7}	0.16×10^{-7}
[NaH_2PO_4]	mol/L	2.332×10^{-3}	0.044×10^{-3}
V (NaH_2PO_4)	mL	0.471	0.004
n(NaH_2PO_4)	mol	10.98×10^{-7}	0.23×10^{-7}
[nanohybrid]$_{NMR}$	mg/mL	26.79	0.32
V(nanohybrid)	mL	0.399	0.004

Quantitative NMR[5] relies on the use of another compound, with signal differing from the compound to be quantified. Such a standard has to be introduced in a well-known concentration in the same concentration range as the tested substance. Therefore, quantification can be deduced by comparing the integrations of the peaks, if the signal-to-noise ratio is higher than 10. Usually, such quantification is achieved by mixing directly the standard in the solution to analyze. However, in some special cases, it can be isolated from the mixture by using a coaxial insert,[6] especially when the standard is not stable in the solvent or reacts with molecules in the solution. In our case, as phosphate and phosphonate have a strong affinity to NP surface, it was decided to use a capillary insert to prevent any troubles. As a standard, we used NaH_2PO_4 compound, which has a distinct ^{31}P signal at 0.08 ppm from that of BzA-TL(PO_3H_2)-$PVCL_{10K}$ expected at around 25 ppm. However, the use of a capillary insert enforces an additional calibration to correct the signal discrepancy between molecules in insert and in solution.

Calibration of the reference

The response of a capillary insert of NaH_2PO_4 in D_2O was calibrated by using a more usual standard for ^{31}P NMR: cyclophosphamide monohydrate placed in D_2O solution of similar concentration in an NMR tube. ^{31}P analysis is shown in figure S16. Integrations were respectively 3.95 and 1 for cyclophosphamide monohydrate and NaH_2PO_4. This benchmarking allowed us to determine a response factor α from the known concentration of standard and the integration of peaks:

$$\frac{n(cyclophosphamide)}{n(NaH_2PO_4)} = \alpha \frac{\int(cyclophosphamide)}{\int(NaH_2PO_4)} \qquad (1)$$

Once the benchmarking validated for the capillary insert of NaH_2PO_4 in D_2O solution, we could then analyze our nanohybrid. A solution of 26.79 mg mL^{-1} of nanohybrid in D_2O was placed inside an NMR tube (table S1).

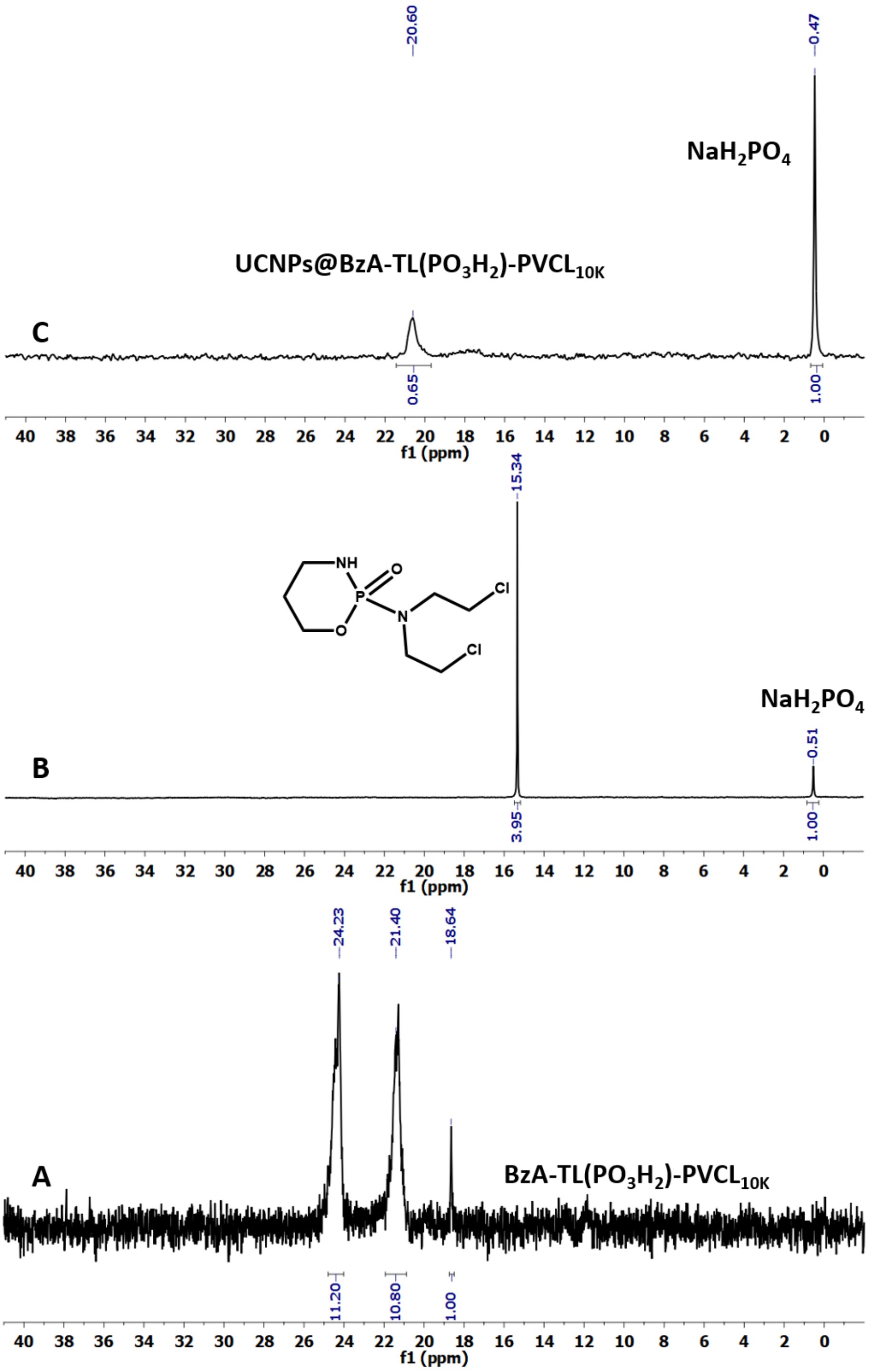

Figure S15. ^{31}P NMR spectra of **(A)** BzA-TL(PO$_3$H$_2$)-PVCL$_{10K}$, **(B)** solution of cyclophosphamide monohydrate with a capillary insert containing D$_2$O solution of NaH$_2$PO$_4$ recorded with the sequence “zgig30” adapted to quantification. **(C)** UCNPs@BzA-TL(PO$_3$H$_2$)-PVCL$_{10K}$ recorded in quantitative conditions (with “zgig30” sequence), with a capillary insert of NaH$_2$PO$_4$ as a standard. (121.49 MHz, D$_2$O, 298K).

The disappearance of the diastereoisomers satellite signals (figure S16) attest to the formation of the nanohybrid and the lack of free polymer.
Therefore, for the quantitative NMR of the nanohybrid, we have:

$$\frac{n(phosphonate)}{n(NaH_2PO_4)} = \alpha \frac{\int(phosphonate)}{\int(NaH_2PO_4)} \qquad (2)$$

$$\frac{n(phosphonate)}{n(NaH_2PO_4)} = \left(\frac{n(cyclophosphamide)}{n(NaH_2PO_4)} \frac{\int(NaH_2PO_4)}{\int(cyclophosphamide)}\right) \frac{\int(phosphonate)}{\int(NaH_2PO_4)}$$

$$n(phosphonate) = n(cyclophosphamide) \frac{\int(phosphonate)}{\int(cyclophosphamide)} \qquad (3)$$

$$n(phosphonate) = n(cyclophosphamide) \times R_I \qquad (4)$$

with $R_I = \frac{\int(phosphonate)}{\int(cyclophosphamide)}$

On both NMR experiments, integrations were respectively normalized by $\int(NaH_2PO_4) = 1$

Integrations on nanohybrid and cyclophosphamide quantitative NMR spectra were respectively independently measured 3 times to provide an average and standard deviation

Table S2. Triplicate independent measurements of integrations on the ^{31}P NMR spectra

	∫(cyclophosphamide)	∫(phosphonate)	$R_I = \frac{\int(phosphonate)}{\int(cyclophosphamide)}$
mesurement 1	3.95	0.65	0.165
mesurement 2	4.4508	0.6343	0.143
mesurement 3	4.35	0.61	0.140
Average	4.250	0.631	**0.149**
Standard deviation	0.265	0.020	**0.013**

The polymer has a single phosphonate group, therefore it can be quantified by ^{31}P NMR:

$$\boldsymbol{n(phosphonate) = n(polymer) = (1.29 \pm 0.12) \times 10^{-7}\ mol} \qquad \mathbf{(5)}$$

D.3. Determination of UCNPs molecular weight for 20nm UCNPs

The UCNP molecular weight was estimated from experimental data gathered in table S3, following the method proposed by Mackenzie *et al.* [7]:

Table S3. Experimental measurement gathered for the 20 nm $NaYF_4$. TEM images were analyzed to get a series of diameter that were all independently used to calculated their corresponding surface and volume using the model of a sphere. The 3 series of distributions (diameter, surface, volume) were analyzed by gaussian fit using Origin Lab, value and error being respectively the average value of the distribution and its full width at half maximum. TOPAS analysis of the XRD diffractogram provided a and c unit cell parameters. Rare earth composition was estimated from the respective amount of precursors introduced in the synthesis. The previous synthesis with similar UCNPs show good agreement with ICP values (data not shown)

	Unit	**value**	**Error σ**
d_{TEM}	Å	200	26
S_{TEM}	$Å^2$	1259.7	317.8
V_{TEM}	$Å^3$	4195800	1583800
a	Å	5.955829	0.0001
c	Å	3.5027819	0.0001
Z(β-$NaREF_4$)		1.5	
M(Na)	g/mol	22.989769	0.00000002
M(F)	g/mol	18.998403	0.0000005
M(Y)	g/mol	88.90585	0.00002
M(Yb)	g/mol	173.04	0.03
M(Tm)	g/mol	168.93421	0.00002
%Y	%	68.87	
%Yb	%	30.11	
%Tm	%	1.02	

The volume of the hexagonal phase can be estimated from the unit cells parameters

$$U_{\beta-NaYF_4} = \frac{2\sqrt{3}}{4} \times a^2 \times c \qquad (6)$$

$$\boldsymbol{U_{\beta-NaYF_4} = 107.604 \pm 0.004}\ \text{Å}^{\mathbf{3}}$$

Knowing the volume of a single UCNP by TEM, it can then be deduced the amount of unit cell per UCNP:

$$N_{unit\ cell/_{NP}} = \frac{V_{TEM}}{U_{\beta-NaYF_4}} \qquad (7)$$

$$\boldsymbol{N_{unit\ cell/_{NP}} = 38993 \pm 14719}$$

The molecular weight of a single unit cell can be calculated knowing the Rare-Earth composition

$$FW_{unit\ cell} = Z \times \big(M(Na) + 4 \times M(F) + (\%Y) \times M(Y) + (\%Yb) \times M(Yb) + (\%Tm) \times M(Tm)\big) \quad (8)$$

$$\boldsymbol{FW_{unit\ cell} = 321.05 \pm 0.03\ g/mol}$$

Eventually, the molecular weight of UCNP can be calculated from (7) and (8):

$$FW_{UCNP} = \boldsymbol{N_{unit\,cell}/_{NP}} \times FW_{unit\,cell} \qquad (9)$$

$$\boldsymbol{FW_{UCNP} = (1.252 \pm 0.473) \times 10^{7}\ g/mol}$$

D.4. Determination of the number of polymer per UCNP

Knowing the mass of the amount of nanohybrid used to prepare the NMR tube and the amount of polymer quantified by NMR, we can deduce the amount of UCNP:

$$m(UCNP) = m(nanohybrid) - m(polymer) \qquad (10)$$

$$m(UCNP) = \left([nanohybrid]_{NMR} \times V_{nanohybrid}\right) - \left(n_{polymer} \times FW_{polymer}\right)$$

$$\boldsymbol{m(UCNP) = (9.400 \pm 0.446) \times 10^{-3}\ g}$$

Knowing the molecular weight of the 20nm UCNP (6), we can then deduce the amount of moles of UCNP.

$$n(UCNP) = \frac{m(UCNP)}{FW_{UCNP}} \qquad (11)$$

$$\boldsymbol{n(UCNP) = (7.51 \pm 2.86) \times 10^{-3}\ mol}$$

Then the amount of polymer per UCNP can be determined from (5) and (11)

$$N_{polymer}/_{NP} = \frac{n_{polymer}}{n(UCNP)} \qquad (12)$$

$$\boldsymbol{N_{polymer}/_{NP} = 172 \pm 67}$$

In average, **there is ≈172 polymer chains anchored at the surface of a single UCNP of 20 nm diameter**

D.5. Determination of polymer to surface Rare Earth ratio

The approximation of the average distance between 2 Rare Earths is estimated from Nadort et al.[8].

$$d_{RE-RE} = \left(\frac{a^{2} \times c \times \frac{\sqrt{3}}{2}}{Z}\right)^{\frac{1}{3}} \qquad (13)$$

$$\boldsymbol{d_{RE-RE} = 34.16 \pm 0.00002}\ \text{Å}$$

Then, the surface of a Rare Earth can be deduced from their interdistance d_{RE-RE}

$$S_{RE} = 4\,\pi \left(\frac{d_{RE-RE}}{2}\right)^2 \qquad (14)$$

$$\boldsymbol{S_{RE} = 54.2385 \pm 0.0003\ \text{Å}^2}$$

By comparing the surface of a Rare Earth (RE) to the surface of a single UCNP measured from the TEM picture, we can then estimate the amount of surface RE per nanoparticle:

$$N_{surface\ RE/_{NP}} = \frac{S_{TEM}}{S_{RE}} \qquad (15)$$

$$\boldsymbol{N_{surface\ RE/_{NP}} = 2323 \pm 586}$$

The density of polymer at the surface of 20nm UCNP can be estimated as the amount of surface Rare Earth per polymer, from (12) and (15):

$$N_{surface\ RE/_{polymer}} = \frac{N_{surface\ RE/_{NP}}}{N_{polymer/_{NP}}} \qquad (16)$$

$$\boldsymbol{N_{surface\ RE/_{polymer}} = 13.5 \pm 6.3}$$

In average, **there is 1 polymer chain for 13.5 surface Rare Earth.**

Then it can be deduced from (14) and (16) the area occupied by one polymer at the surface of one UCNP:

$$S_{one\ polymer\ chain\ at\ the\ surface} = S_{RE} \times N_{surface\ RE/_{polymer}} \qquad (17)$$

$$\boldsymbol{S_{one\ polymer\ chain\ at\ the\ surface} = 732 \pm 341\ \text{Å}^2 = 7.32 \pm 3.41\ \mathbf{nm}^2}$$

Then the density of polymer at the surface can be deduced from (17):

$$Polymer\ density = \frac{1}{S_{one\ polymer\ chain\ at\ the\ surface}} \qquad (18)$$

$$\boldsymbol{Polymer\ density = 0.14 \pm 0.06\ molecule/nm^2}$$

This is in agreement with the literature. Ute Resch-Genger group estimated 4 molecule/nm^2 for alendronate, which has a way less steric hindrance than such a polymer stabilizer used in our study.[9]

D.6. Estimation of the amount of polymer per particle on ultrasmall (US) UCNPs

Table S4. Experimental measurement gathered for the ultrasmall UCNPs. TEM images were analyzed to get a serie of diameter that were all independently used to calculated their corresponding surface and volume using the model of a sphere. The 3 series of distributions (diameter, surface, volume) were analyzed by gaussian fit using Origin Lab, value and error being respectively the average value of the distribution and its FWHM. TOPAS analysis of the XRD diffractogram provided a and c unit cell parameters.

	Unit	Value	Error σ
D_{US}	Å	58	11
S_{US}	Å^2	1.057×10^4	0.283×10^4
a_{US}	Å	6.0190026	0.0001
c_{US}	Å	3.5805707	0.0001
Z(β-NaREF$_4$)		1.5	

Similarly to (13) it can be calculated the average distance between 2 lanthanides in the ultrasmall UCNPs:

$$d_{(RE-RE)_{US}} = \left(\frac{{a_{US}}^2 \times c_{US} \times \frac{\sqrt{3}}{2}}{Z} \right)^{\frac{1}{3}} \qquad (19)$$

$$\boldsymbol{d_{(RE-RE)_{US}} \approx 4.2152} \text{ Å}$$

From this, it can be deduced a surface occupied by a single lanthanide:

$$S_{(RE)_{US}} = 4\,\pi \left(\frac{d_{(RE-RE)_{US}}}{2} \right)^2 \qquad (20)$$

$$\boldsymbol{S_{(RE)_{US}} \approx 55.218} \text{ Å}^2$$

Therefore, the amount of Rare Earth at the surface of the ultrasmall UCNP (US NP) can be estimated as:

$$N_{surface\ RE/_{US\ NP}} = \frac{S_{US}}{S_{(RE)_{US}}} \qquad (21)$$

$$\boldsymbol{N_{surface\ RE/_{US\ NP}} \approx 189}$$

It can be deduced the area occupied by one polymer at the surface of a single UCNP

$$S_{(polymer)_{patch}} = N_{surface\ RE/_{polymer}} \times S_{(RE)_{US}} \qquad (22)$$

$$\boldsymbol{S_{(polymer)_{patch}} \approx 732}\ \text{Å}^{\mathbf{2}}$$

It can be then deduced the radius of the “polymer disk.”

$$r_{(polymer)_{patch}} = \sqrt{\frac{S_{(polymer)_{patch}}}{4\pi}} \qquad (23)$$

$$\boldsymbol{r_{(polymer)_{patch}} \approx 7.63}\ \text{Å}^{\mathbf{2}}$$

The compacity of a hexagon is 0.9. Therefore, the effective surface occupied by polymer patches is

$$S_{(polymer)_{effective}} = 0.9 \times S_{(polymer)_{patch}} \qquad (24)$$

$$\boldsymbol{S_{(polymer)_{effective}} \approx 664}\ \text{Å}^{\mathbf{2}}$$

$$OM^2 = r_{(polymer)_{patch}}{}^2 + \left(r_{(polymer)_{patch}} + \frac{d_{US}}{2}\right)^2 \qquad (25)$$

$$\tan(\vartheta) = \frac{r_{(polymer)_{patch}}}{r_{(polymer)_{patch}} + \frac{d_{US}}{2}}$$

$$\tan(\vartheta) \approx 0.33$$

$$\boldsymbol{\vartheta = Arctan(\vartheta) \approx 0.32} \qquad (26)$$

Packing model 1: considering all cones tangent to each other.

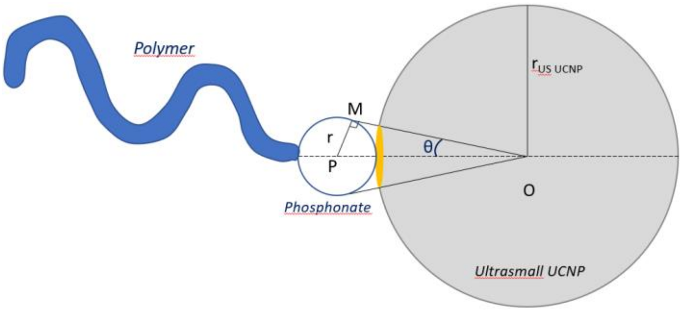

Scheme S2. Packing model 1

The area of the spherical cap can be expressed by:

$$\left(S_{spherical\ cap}\right)_{model\ 1} = 2\pi \times \left(\frac{d_{US}}{2}\right)^2 \times (1 - \cos(\vartheta)) \qquad (27)$$

$$\boldsymbol{\left(S_{spherical\ cap}\right)_{model\ 1} \approx 272}\ \text{Å}^{\mathbf{2}}$$

$$\left(N_{polymer}/_{US\ UCNP}\right)_{model\ 1} = 2 \times (1 - \cos(\vartheta)) \qquad (28)$$

$$\boldsymbol{\left(N_{polymer}/_{US\ UCNP}\right)_{model\ 1} \approx 40}$$

Packing model 2: considering UCNP as a truncated icosahedron (model of a soccer ball).

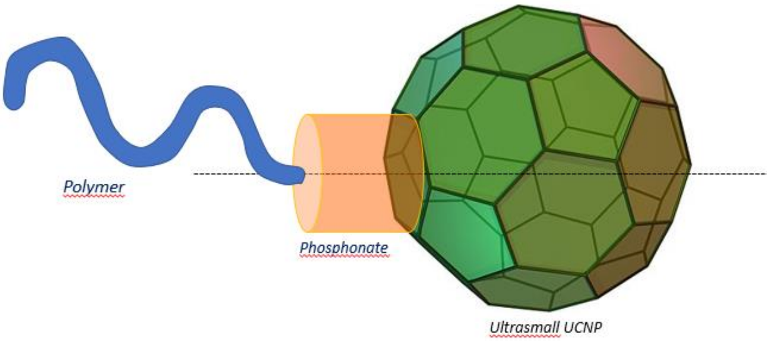

Scheme S3. Packing model 2.

The surface of such a truncated icosahedron consists of 12 pentagons and 20 hexagons. Thus, the disk limiting the spherical cap can be defined with the area:

$$\left(S_{spherical\ cap}\right)_{model\ 2} = \pi \times \left(\frac{d_{US}}{2} \times (\sin(\vartheta))\right)^2 \qquad (29)$$

$$\boldsymbol{\left(S_{spherical\ cap}\right)_{model\ 2} \approx 265}\ \text{Å}^{\mathbf{2}}$$

A similar surface of the spherical cap is obtained form these 2 first packing models, giving a similar density of around 40 polymer chains/UCNP

Packing model 3: Packing of sphere/rods on a sphere

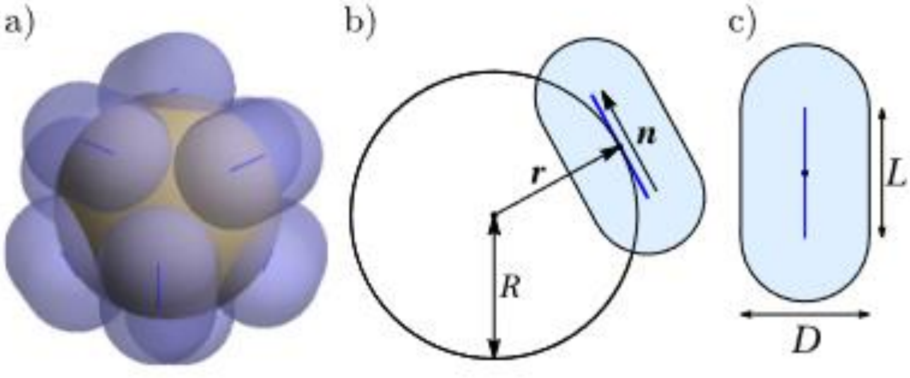

Scheme S4. The model reproduced from ref [10].

From the above-mentioned ϑ angle, we can determine the aperture 2ϑ

$$(2\vartheta)_{rad} \approx \mathbf{0.64\ rad} \qquad (30)$$

This can be converted into a separation angle in degrees:

$$2\vartheta = (2\vartheta)_{rad} \times \frac{360}{2\pi}$$

$$\boldsymbol{2\vartheta \approx 36.9\ ^\circ}$$

Optimal packing onto a sphere has been theoretically modelised and calculated in 3D space by N. J. A. Sloane.[11] Using this simulation as an abaque, we can extract the amount of spherical cap that can be arranged, knowing the minimal angle $2\vartheta = 36.9°$: 32.5 packed spheres. As a result, around 32.5 polymers can be anchored onto a single ultrasmall UCNP. Interestingly this value does not differ too much compared to the two previous models.

E. Colloidal stability in different solvent

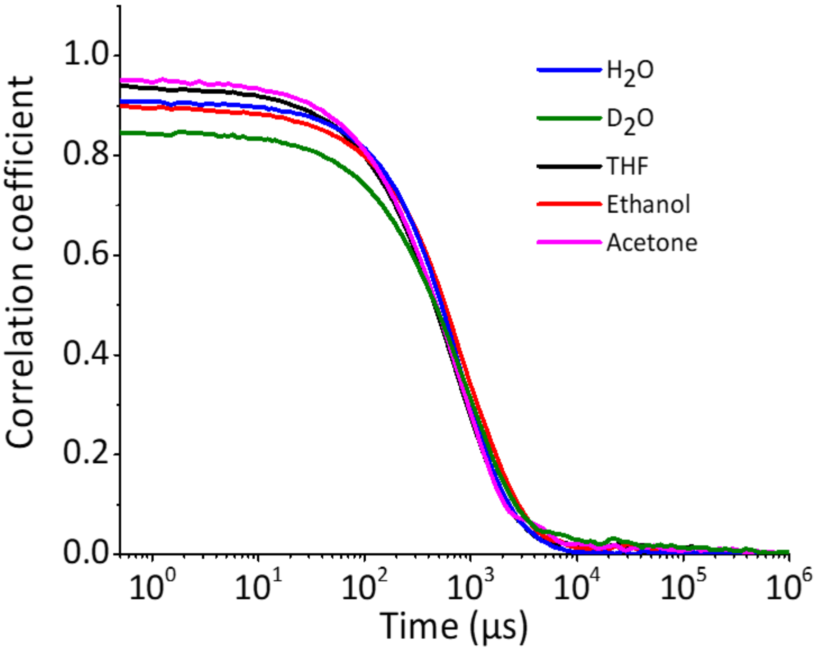

Figure S16. Correlograms of UCNPs@BzA-TL(PO_3H_2)-PEG_{2K} dispersed in different solvents

References

1 Z. Li and Y. Zhang, *Nanotechnology*, 2008, **19**, 345606.

2 B. Amouroux, C. Roux, J.-D. Marty, M. Pasturel, A. Bouchet, M. Sliwa, O. Leroux, F. Gauffre and C. Coudret, *Inorg. Chem.*, 2019, **58**, 5082–5088.

3 B. Amouroux, Nanoparticules upconverting : vers la microscopie en super-résolution,These de doctorat, Université Toulouse III, 2019.

4 X. Zhai, Y. Wang, X. Liu, S. Liu, P. Lei, S. Yao, S. Song, L. Zhou, J. Feng and H. Zhang, *ChemPhotoChem*, 2017, **1**, 369–375.

5 U. Holzgrabe, *Prog. Nucl. Magn. Reson. Spectrosc.*, 2010, **57**, 229–240.

6 T. J. Henderson, *Anal. Chem.*, 2002, **74**, 191–198.

7 L. E. Mackenzie, J. A. Goode, A. Vakurov, P. P. Nampi, S. Saha, G. Jose and P. A. Millner, *Sci. Rep.*, 2018, **8**, 1106.

8 A. Nadort, J. Zhao and E. M. Goldys, *Nanoscale*, 2016, **8**, 13099–13130.

9 E. Andresen, C. Würth, C. Prinz, M. Michaelis and U. Resch-Genger, *Nanoscale*, 2020, **12**, 12589–12601.

10 F. Smallenburg and H. Löwen, *J. Chem. Phys.*, 2016, **144**, 164903.

11 Spherical Codes, http://neilsloane.com/packings/, (accessed August 2, 2021).